CM² MAGAZINE

第 33 期

南方科技大学海洋磁学中心主编

创刊词

海洋是生命的摇篮，是文明的纽带。地球上最早的生命诞生于海洋，海洋里的生命最终进化成了人类，人类的文化融合又通过海洋得以实现。人因海而兴。

人类对海洋的探索从未停止。从远古时代美丽的神话传说，到麦哲伦的全球航行，再到现代对大洋的科学钻探计划，海洋逐渐从人类敬畏崇拜幻想的精神寄托演变成可以开发利用与科学研究的客观存在。其中，上个世纪与太空探索同步发展的大洋科学钻探计划将人类对海洋的认知推向了崭新的纬度：深海（deep sea）与深时（deep time）。大洋钻探计划让人类知道，奔流不息的大海之下，埋藏的却是亿万年的地球历史。它们记录了地球板块的运动，从而使板块构造学说得到证实；它们记录了地球环境的演变，从而让古海洋学方兴未艾。

在探索海洋的悠久历史中，从大航海时代的导航，到大洋钻探计划中不可或缺的磁性地层学，磁学发挥了不可替代的作用。这不是偶然，因为从微观到宏观，磁性是最基本的物理属性之一，可以说，万物皆有磁性。基于课题组的学科背景和对海洋的理解，我们对海洋的探索以磁学为主要手段，海洋磁学中心因此而生。

海洋磁学中心，简称 CM^2，一为其全名“Centre for Marine Magnetism”的缩写，另者恰与爱因斯坦著名的质能方程 $E = MC^2$ 对称，借以表达我们对科学巨匠的敬仰和对科学的不懈追求。

然而科学从来不是单打独斗的产物。我们以磁学为研究海洋的主攻利器，但绝不仅限于磁学。凡与磁学相关的领域均是我们关注的重点。为了跟踪反映国内外地球科学特别是与磁学有关的地球科学领域的最新研究进展，海洋磁学中心特地主办 CM^2 Magazine，以期与各位地球科学工作者相互交流学习、合作共进！

“海洋孕育了生命，联通了世界，促进了发展”。 21 世纪是海洋科学的时代，由陆向海，让我们携手迈进中国海洋科学的黄金时代

目 录

岩石磁学演绎

第 23 章　地磁场相对古强度（Relative paleointensity, RPI）

对于火山岩，我们可以在实验室模拟 TRM 过程，在已知 H_0 下获得实验室 TRM，并推算地磁场古强度。

对于沉积物，如果我们也能在实验室模拟 DRM 获得过程，在已知 H_0 下获得 DRM，是否也能推算地磁场古强度？

理论上讲，如果我们能够完美地模拟自然界的沉积过程，应该能够达到这一目的。可是，实际情况要比这个复杂得多。第一个就是沉积后的压实过程。除了沉积，DRM 要想被锁定，需要压实过程，这个在实验室很难被完美模拟。第二个就是沉积环境中的离子浓度。不同的离子浓度对 DRM 结果影响很大，我们并不清楚自然沉积物沉积时具体的沉积环境参数。总之，在实验室进行一些 DRM 的简单模拟还是可行的，但是无法达到 TRM 这样完美的模拟程度，所以到目前为止，还不能利用 DRM 来确定绝对的地磁场古强度，不过这倒是一个可以发展的方向。

但是 DRM 确实和地磁场强度密切相关。一般情况，地磁场强度越大，DRM 也就越大。但是，还有一个因素需要考虑，那就是磁性颗粒的含量。显然磁性矿物颗粒的含量越高，样品的整体剩磁就会越高。

因此，一块沉积物样品的 DRM 和地磁场强度、磁性矿物含量都相关。要想突出地磁场的影响，就必须要把磁性矿物含量的影响压制。

目前我们所提及的大部分磁性参数（χ、SIRM、ARM）除了受含量影响，都和磁性矿物的粒径密切相关。M_s 确实只代表含量，但是想要获得 M_s 就需要测量磁滞回线，所需实验量很大，但是，M_s 作为 RPI 的磁性矿物含量指标，需要系统的研究。

最终，大家还是选用 χ、SIRM 和 ARM 作为最常见的磁性矿物含量替代指标，前提是，磁性矿物的粒径变化不大。

磁畴状态与粒径相关，所有确定磁畴状态的实验，在这里都可以派上用场，磁滞回线参数、FORC 等。还有一种更为便捷的方法就是做以上几种参数的相关图。如果它们之间都具有很好的线性正相关关系，这就说明磁性矿物的粒径变化不大，从而主要代表含量变化，可以被用来确定 RPI。

磁性矿物的性质一定会变化，因为它们还代表着气候因子。全球气候在轨道周期尺度上变化，随之磁性矿物的物源、传输路径、保存状态等等都会受到影响。于是，Lisa Tauxe 教授提出，只要磁学性质的变化范围不超过一个数量级（10 倍），就认为可以被用来进行构建 RPI 曲线。

大家会问，为什么是一个数量级，而不是其它的阀门值？事实上，这个数值确实有一点随机。如果只是含量的变化，影响会小些。如果是粒径在大幅度变化，情形就复杂了。所以不能一概而论，也不能拿这个阀门值当尚方宝剑。

好了，我们来到了重点，到底如何确定 RPI？

最简单的方法就是用归一化的方法：

RPI = DRM / 含量参数

一般情况下，我们会同时测量 χ、SIRM 和 ARM。这样就会得到三条 RPI 曲线，可以相互验证。

总的说来磁化率更为复杂，而 SIRM 和 ARM 相对好些，因为 SIRM 和 ARM 与 DRM 一样是剩磁，性质更类似。

为了进一步去除一些软磁（矫顽力较小）成分的影响，古地磁学家发展出了稍微复杂的 RPI 确定方法。对 DRM 和 ARM 以及 SIRM 都做逐步 AF 退磁处理，然后做 DRM 和 ARM，以及 DRM 和 SIRM 的相关曲线，在高场部分做线性拟合，这就避免了低场 VRM 的影响，以及测量的误差问题。

这样做的实验量会增加，但是结果会更可信。

经过这些实验，我们得到了一条所谓的 RPI 曲线，它一定会高高低低变化，这些特征代表真实的地磁场变化吗？

这个问题还真不是一个很简单的问题。

我们首先想到的是 DRM 被分母归一化之后，会不会受到分母的调制作用？也就是说所谓 RPI 变化可能是由于分母的变化造成的。在这种情况下，RPI 和其归一化参数之间就会存在相关性。目前比较流行的方法是做两者之间的频率谱相

关性检测。如果二者的频率谱不相关，这就说明归一化参数的变化并没有引起二者的 RPI 特征变化，那么 RPI 的变化特征就更倾向于是地磁场信息。

为了进一步加强曲线的可靠性，另外一个方法就是在不同区域多构建几条同一时段的 RPI 曲线，如果大家长得都非常相似，就可以相互验证曲线信息的可靠性。

要想得到完全一样的曲线，那是不可能完成的任务。不同的曲线其时间框架都存在误差，沉积环境也不一样，有的地方非偶极子场的影响很显著。林林总总的因素加在一起，使得不同地区的曲线总是存在一些不一致的情况。这也难不倒科学家，他们采用了一种叫做 Bootstrap stacked 的方法，合成一条标准曲线，同时还有误差分布信息。

Bootstrap 被前人亲切地翻译为“解靴带法”。对于一种数学算法，更准确的意思应该是自适应法，或者自助法，这是一种抽样方法，对小样本非常有效。RPI 研究为什么用 Bootstrap 方法来进行统计？因为样本数太少，经过不同学者一二十年的研究，能够得到一二十条统一时段的 RPI 曲线就不错了。

经过上面的各种努力，我们获得了一条所谓的标准 RPI 曲线，而且有误差分布，这下总可以认为可以代表地磁场的相对变化特征了吧！

且慢，这还需要其他方法得到的地磁场古强度数据验证。比如，虽然用火山岩获得的地磁场绝对古强度是零星分布的，但是有总是比没有好。如果 RPI 曲线和绝对强度曲线变化很一致，这就进一步增加了 RPI 的可信度。对于长序列的 RPI 曲线，就需要和洋壳获得的磁化强度变化曲线来对比了。

还有一种信息也非常有效，那就是宇宙核素，比如 ^{10}Be 含量的变化。地磁场是地球的保护伞。地磁场强度高的时候，宇宙射线难以到达地球大气层，导致 ^{10}Be 生产效率较低。反之，^{10}Be 的含量就会高。也就是说地磁场强度和 ^{10}Be 含量之间具有反相关关系。

测量 ^{10}Be 和 ^{9}Be 可没那么容易。目前只有几个大型加速器实验室能做这样的测量，产出的曲线并不多。但是，有限的结果显示，^{10}Be 数据和 RPI 数据确实有反相关关系，佐证了 RPI 的可靠性。

通过对比 ^{10}Be 和 RPI 曲线，我们还可以用来估算 DRM 的 Lock-in 深度。Lock-in 过程相当于一个低通滤波过程。我们的曲线可以被分解为不同波长（频

率）和幅度的成分，通过简单的快速傅里叶变化（FFT）就可以实现。所谓的滤波器就是只让一定频率的成分通过，其它成分都被压抑。噪音属于高频信息，所以低通滤波器就可以把这些噪音压制。

对于古地磁记录，在沉积物慢慢压实的过程中，产生低通滤波效果。那些高频成分就无法被记录，信号的强度会降低，同时古地磁信息会向下移动，让信息偏老。但是 ^{10}Be 就不需要经过这样的过程。

当然，这两种信息都会受到 SML 的影响。SML 和 Lock-in 还是有着本质区别的。前者虽然也会让古地磁信息记录向下移动几公分，但不是低通滤波器。

如果我们详细考察 ^{10}Be 峰值和 RPI 低值之间的深度关系，就会发现二者经常错位，其错开的厚度就是所谓的 Lock-in 深度。

我们假设 Lock-in 深度都是 15 cm。对于一个快速堆积的沉积物层来说，这个影响会很小。但是对于沉积速率很慢的沉积物来说，15 cm 可能就代表着很长的时间。当把深度转换为时间后，就会发现古地磁记录被向下移动了很多，造成了不同剖面之间古地磁信息（比如古地磁极性倒转边界）无法准确横向对比。

CM2 研究进展

140 千年以来亚北极太平洋地区一直存在地磁场非偶极子行为吗？

地磁场产生于地球液态外核磁流体运动，蕴含着丰富的地球内部动力学过程。此外，它可以有效地屏蔽宇宙射线，对地球环境和生命演化至关重要。目前，对地磁场非偶极子成分的研究还很薄弱，尤其在亚北极太平洋地区缺乏高精度的可靠记录。本文研究了采自西北太平洋底特律火山的沉积物钻孔 LV63-4-2 (5.25 m)，通过综合放射性绝对年代、氧同位素及古生产力指标和火山玻璃等指标，建立了该孔 140 ka 年代学框架。在此年代框架基础上，我们进一步构建了该区域地磁场相对古强度（RPI）演化曲线。整体上，亚北极地区 RPI 记录与全球 RPI 记录具有很好的一致性，但同时也存在明显的局部异常，比如在 64-70 ka 出现地磁倾角异常，以及在~12 ka 出现显著的 RPI 峰值。我们认为，这些现象与东亚磁通量高异常有关，表明在高纬度地区核幔边界存在一个持续性的磁通量异常，这为正确解释东亚以及北太平洋地区地磁场非偶极子特征提供了模型基础，该成果已在 Science Bulletin 最新发表 https://doi.org/10.1016/j.scib.2020.05.016

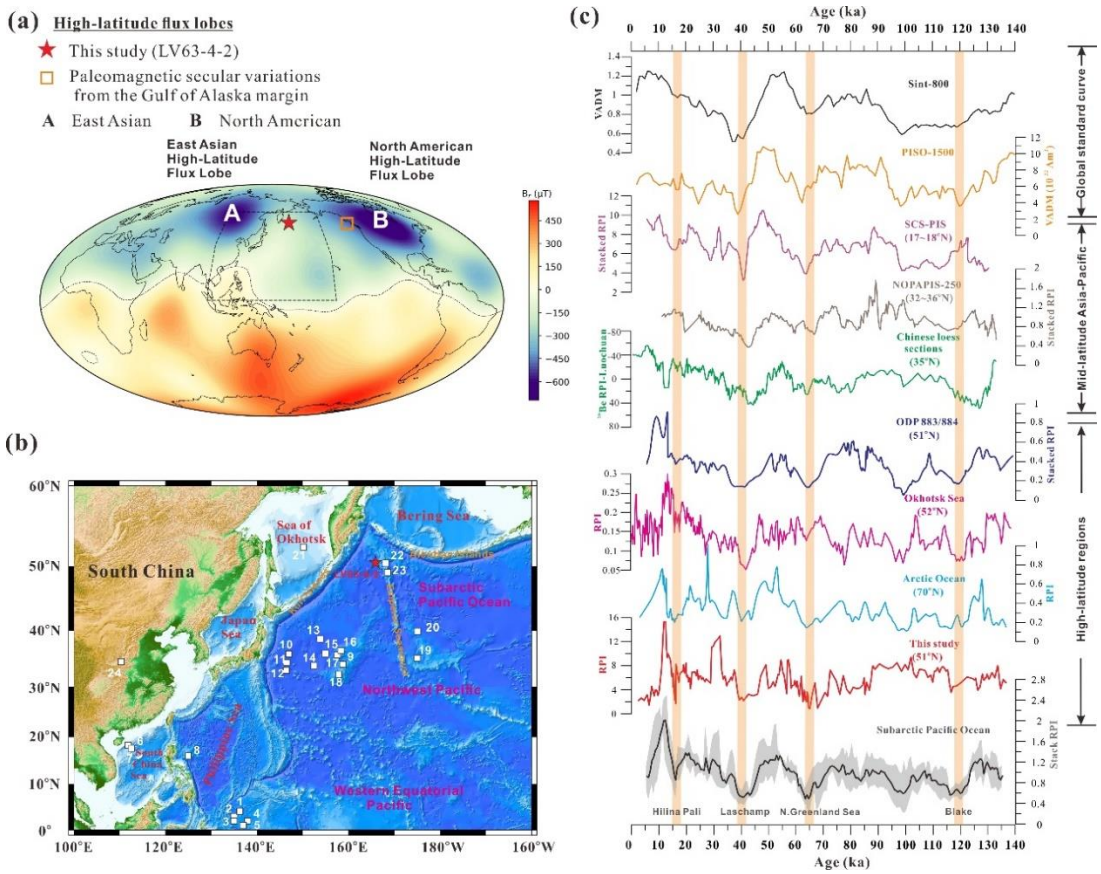

文献导读

1. 育公河流袭夺对周边地形的影响受控于晚新生代的气候变化

翻译人：仲义 zhongy@sustech.edu.cn

Bender. A. M., Lease R.O., Corbett, L. B., et al., ***Late Cenozoic climate change paces landscape adjustments to Yukon River capture*** *[J]. Nature Geoscience, 208, 10263.*

https://doi.org/10.1038/s41561-020-0611-4.

摘要：晚新生代变冷和改变在冰期-间冰期的旋回节律被认为是~3 Ma 以来全球侵蚀速率增强的主要原因。在大多数地形中基岩河流的侵蚀速率和模式与晚新生代气候变化的响应仍然存在争议。本文中作者基于放射性同位素及光释光定年的方法，对沿着育公河流盆地中“41英里河流”的基岩阶地，重建了 5 Ma 以来受到晚新生代气候体系与 2.6 Ma 育公河上游河流袭夺的河流演化历史。育公河流袭夺后导致“41 英里河流”出水口下降，随后对“41 英里河流”盆地分别在 2.4-1.8 Ma 和~1 Ma 发生两次巨大的脉冲式基岩侵入。而这些河流袭夺直接破坏了较长的缓慢河道的沉积间断，这与 4.8-2.4 Ma 和 1.8 到~1Ma 之间的气候变化近乎一致。从 4.3 Ma 以来“41 英里河流”输送到白令海的物源和堆积速率的改变与观测到河流侵夺的变化一致。我们的结果将河流冲积和袭夺作用与晚新生代气候稳定性与变化相互结合，进一步证实气候变化改变降水和径流变化从根本上控制着河流袭夺和地形侵蚀的假设。

ABSTRACT: Late Cenozoic cooling and changes in glacial–interglacial cycle tempo are thought to increase global rates of erosion starting ~3 million years ago (Ma). Bedrock rivers set rates and patterns of erosion in most landscapes, but constraints on river response to late Cenozoic climate change remain elusive. Here, we determine cosmogenic isotope and luminescence ages of well-preserved bedrock terraces along the Fortymile River (Yukon River basin) to reconstruct an ~5 Myr history of fluvial adjustment to late Cenozoic climate and Yukon River headwater capture at 2.6 Ma. Post-capture Yukon River downcutting lowered the Fortymile River outlet, forcing subsequent bedrock incision throughout the Fortymile basin in two pulses, from 2.4 to 1.8 Ma and at ~1 Ma. These pulses of incision disrupted longer intervals of slow river channel sedimentation under near-consistent climate forcing from 4.8 to 2.4 Ma and from 1.8 to ~1 Ma. The Fortymile River delivers sediment to the Bering Sea, where provenance and accumulation rate changes since 4.3 Ma match

observed variations in incision. Our results link alluviation and incision to late Cenozoic climate steadiness and change, respectively, and support the hypothesis that climate-forced changes in precipitation and runoff fundamentally control the pace of river incision and landscape erosion.

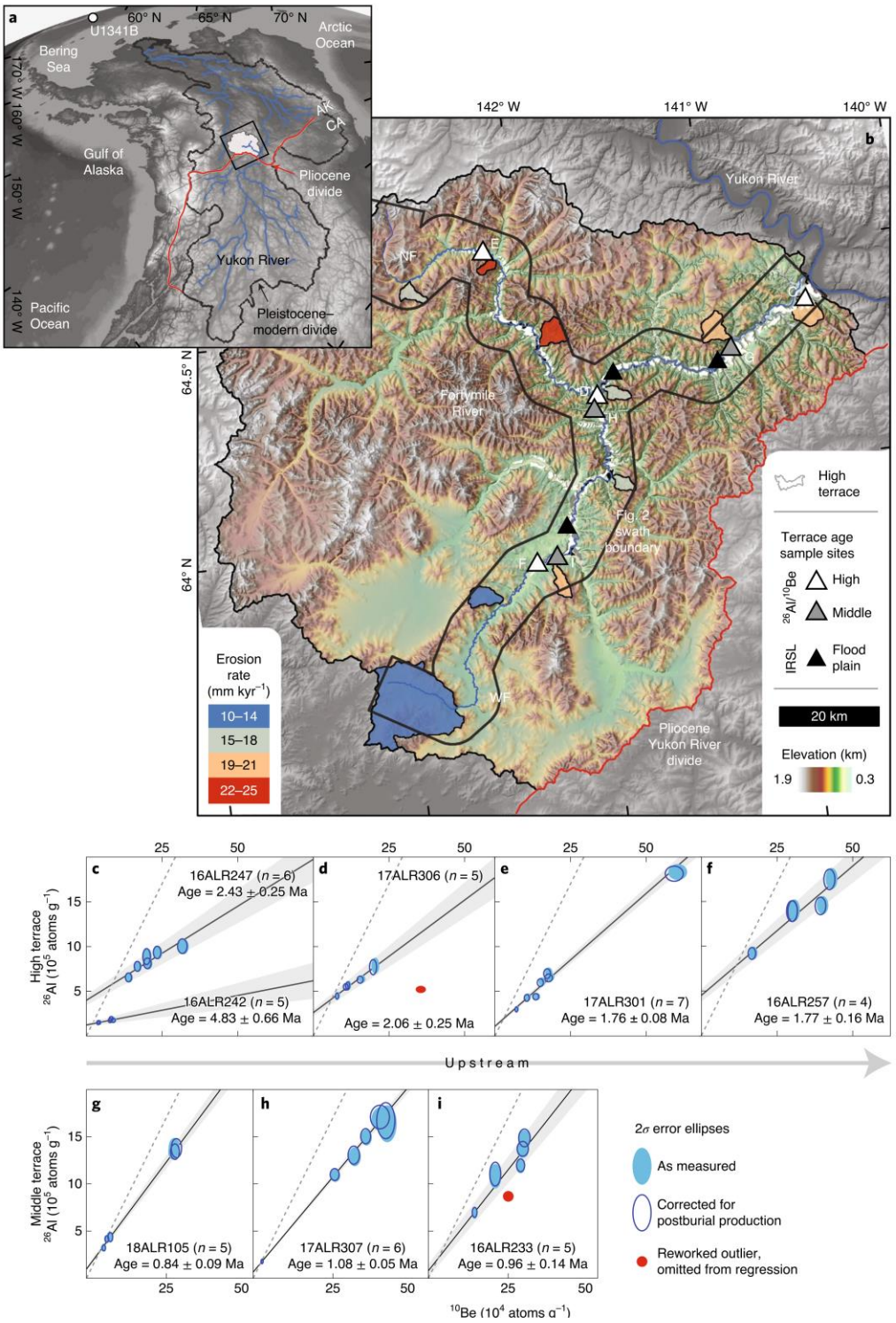

Figure 1. Fortymile River setting and cosmogenic results. a, Oblique northwest view of Fortymile River basin (white polygon), Yukon River basin, captured Pliocene divide and adjacent ocean basins. b, Fortymile River geomorphic map, sample locations and cosmogenic ^{10}Be-based erosion rates. IRSL ages

of floodplain sand range from 5 to 2 ka. c–i, Cosmogenic $^{26}Al/^{10}Be$ isochron burial age plots. The dashed grey line is the $^{26}Al/^{10}Be$ surface production ratio and ~zero age. Regression uncertainties are 1σ.

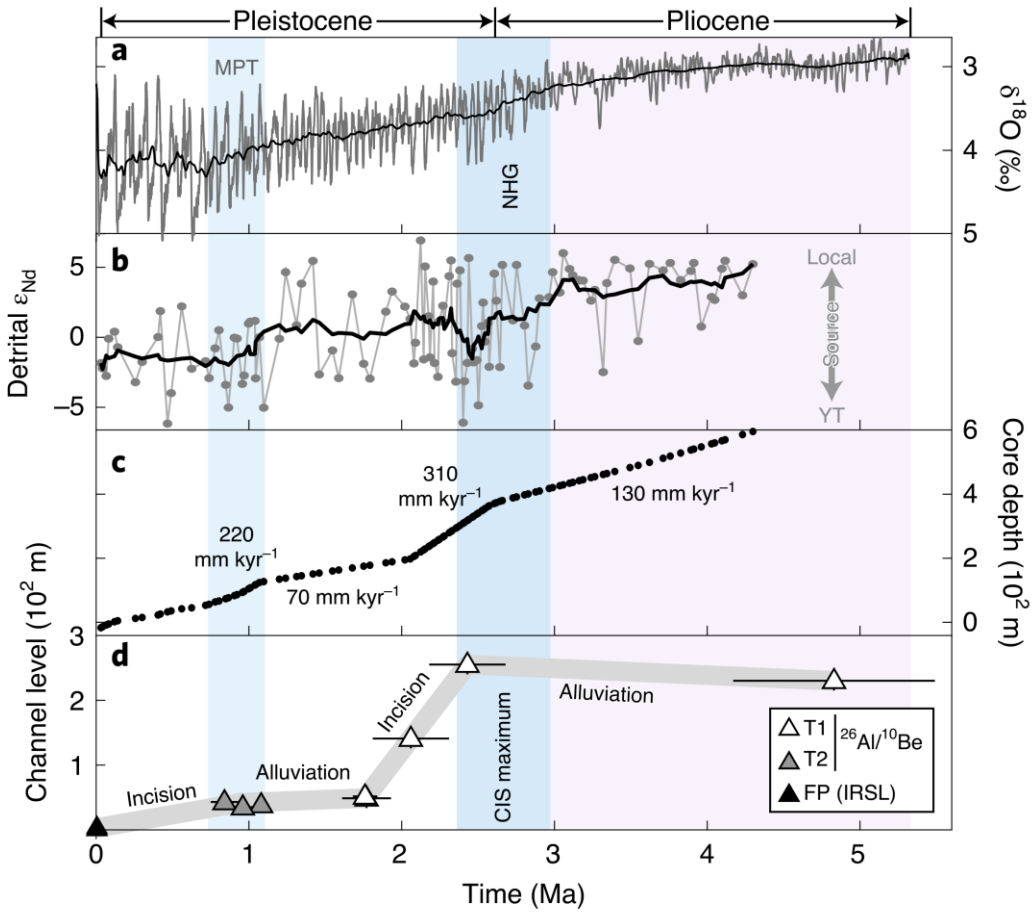

Figure 2. Late Cenozoic variations in climate, Bering sea sedimentation and Fortymile River incision. **a**, Global benthic $\delta^{18}O$, the black line depicts the 105-yr moving average. **b**, Detrital εNd values from Integrated Ocean Drilling Program (IODP) Site U1341B in the Bering Sea; more negative values reflect increased Yukon-Tanana Upland (YT) sedimentary provenance. **c**, Age–depth model for IODP Site U1341B from biostratigraphy, magnetostratigraphy and astronomically tuned chemostratigraphy; detrital sediment fraction is ~40 weight %. **d**, Cosmogenic $^{26}Al/^{10}Be$ isochron burial ages of T1 and T2 and IRSL ages plotted against height above the mid–late Holocene-aged floodplain (FP). CIS maximum extent coincides with the onset of widespread Northern Hemispheric glaciation (NHG) and marks the timing of Yukon River capture; mid-Pleistocene climate transition (MPT) from ~40 to ~100 kyr glacial–interglacial cycles.

2. 微量元素作为古环境指标：为什么要对沉积速率说明？

翻译人：蒋晓东 jiangxd@sustech.edu.cn

Crombez V, Rohais S, Euzen T, er al. ***Trace metal elements as paleoenvironmental proxies: Why should we account for sedimentation rate variations ?*** *[J].* ***Geology****, 2020, 48, 839-843. https://doi.org/10.1130/G47150.1*

摘要：

微量元素通常用于富有机质环境中进行古环境重建。例如，受控于初级生产力和氧化还原条件变化的微量元素用于古环境研究。近期，这些指标在古环境研究中受到热捧，并用于大尺度范围（10-100km）研究中。然而，在盆地范围应用这些地球化学指标时，如果忽略沉积速率的话可能引起古环境条件解译的偏差。本研究发现，沉积速率可影响地球化学记录，引起微量元素解译的偏差。基于沉积速率，我们对加拿大西部三叠纪上蒙特尼组多伊格磷酸盐（Upper Montney Formation and Doig Phosphate）进行研究，计算了自生部分关键微量元素的的堆积速率，以此校正阿根廷侏罗-白垩纪瓦卡穆尔塔组（Vaca-Muerta Formation (Jurassic–Cretaceous, Argentina）的微量元素含量。研究发现相较于惯常的微量元素结果，沉积速率校正的微量元素具有不同的古环境解释。元素富集通常指示缺氧的沉积环境，但可能反应了低的沉积速率和沉积区间的压缩。本研究也引入了一个新的工作流程解译盆地范围长时间尺度古环境研究中的沉积速率。

ABSTRACT： Trace metal elements (TMEs) are commonly used to reconstruct the environmental conditions present during the deposition of organic-rich sediments. For example, TME concentrations controlled by changes in primary productivity and redox conditions are widely used in paleoenvironmental studies. Recently, these proxies have undergone a resurgence of interest and are commonly used in large-scale (10–1000 km) studies. However, applying these geochemical proxies at basin scale while ignoring variations in sedimentation rates (SR) may lead to misinterpretation of paleoenvironmental conditions. Here, we show how SR can affect the geochemical records and may lead to incorrect interpretations of TME evolution. Accounting for SR, we computed the authigenic fraction accumulation rates of key TMEs in the Upper Montney Formation and Doig Phosphate (Triassic, western Canada), and we correct the concentration of these elements in the Vaca-Muerta Formation (Jurassic–Cretaceous, Argentina). Our SR-corrected TME

proxies require a different interpretation of paleoenvironmental conditions (e.g., primary productivity, basin restriction) compared to conventional TME results and highlight that elementary enrichments commonly interpreted as indicative of anoxic depositional environments may reflect low SR and the formation of condensed intervals. This work also introduces a new workflow to account for SR in paleoenvironmental studies at basin scale and over long time periods.

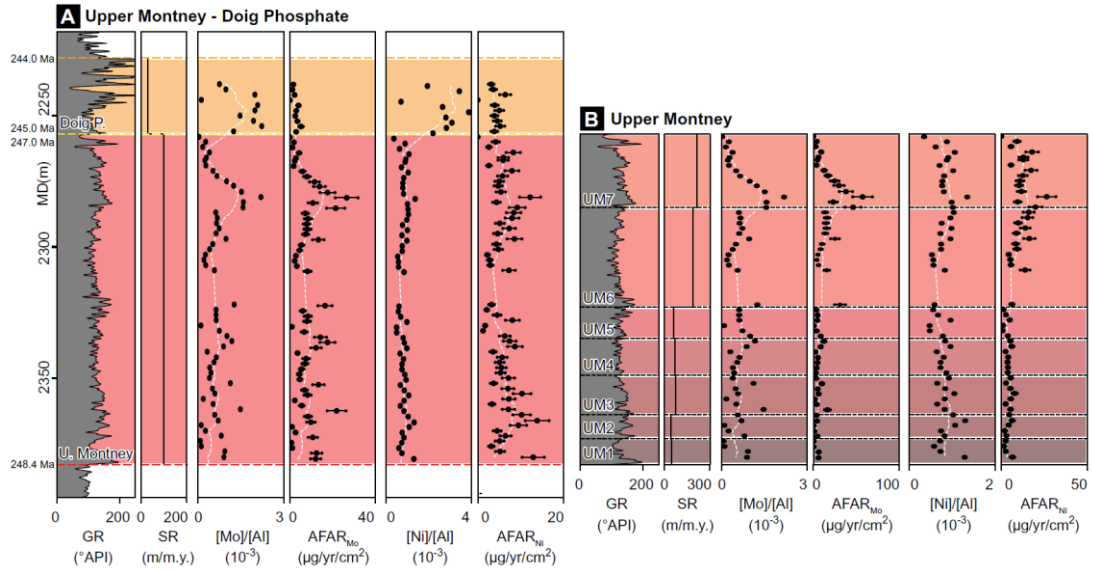

Figure 1. Gamma ray (GR), sedimentation rate (SR), trace metal element (TME) ratios, and authigenic fraction accumulation rates (AFAR) of Mo and Ni in the Upper Montney Formation and Doig Phosphate, western Canada. AFAR values are presented with confidence interval accounting for ±20% incertitude in SR. (A) Variation of TME proxies and Mo and Ni AFAR across the Upper Montney–Doig Phosphate boundary. (B) Variations of proxies within the Upper Montney Formation, considering high-resolution SR changes across seven parasequences. In B, duration of each parasequence is estimated to be 0.2 m.y. (Euzen et al., 2018). White dash lines represent moving average on five samples. MD—measured depth.

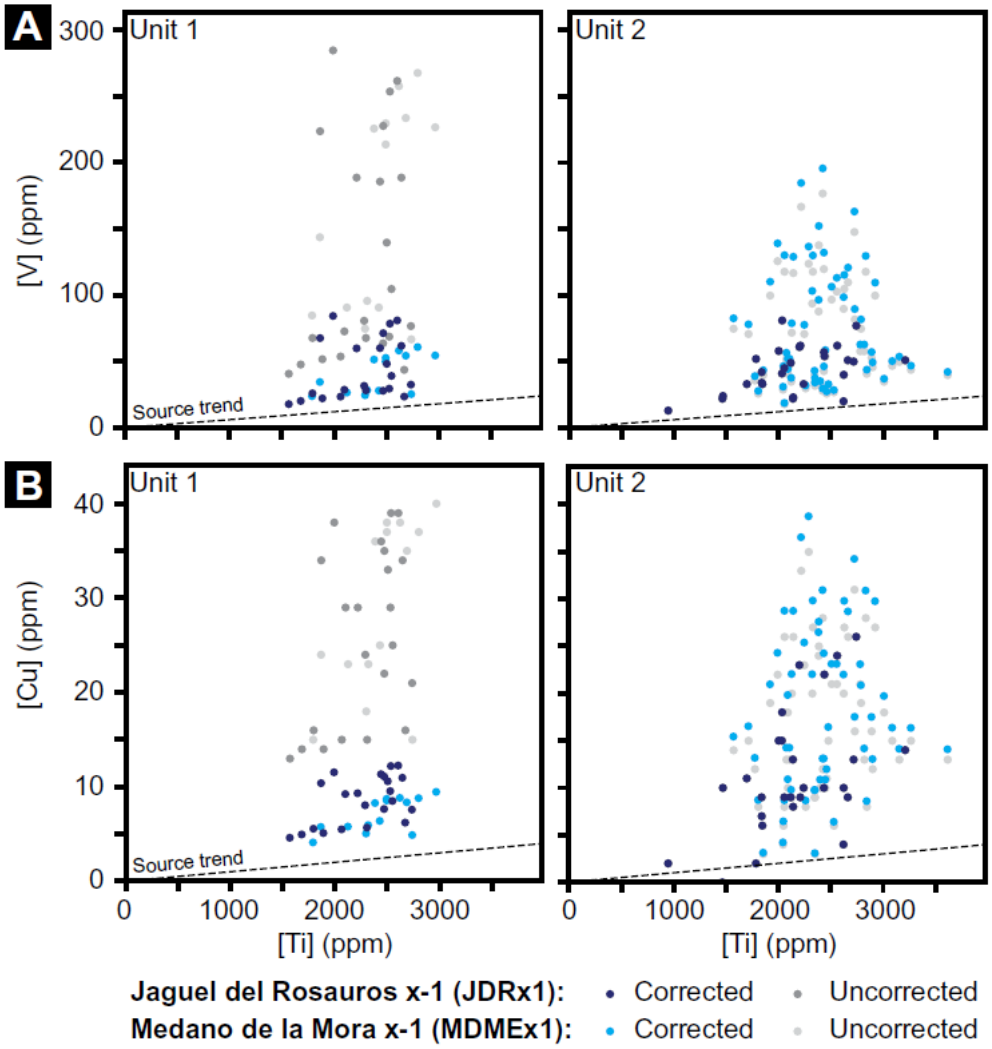

Figure 2. Scatter plots of V versus Ti (A) and Cu versus Ti (B) in units 1 and 2 of the Vaca-Muerta Formation (Argentina) from two wells. Uncorrected data are shown in shades of gray, and corrected elementary concentrations are shown in shades of blue. Here, source trends are identical between wells to reflect same nature of detrital material.

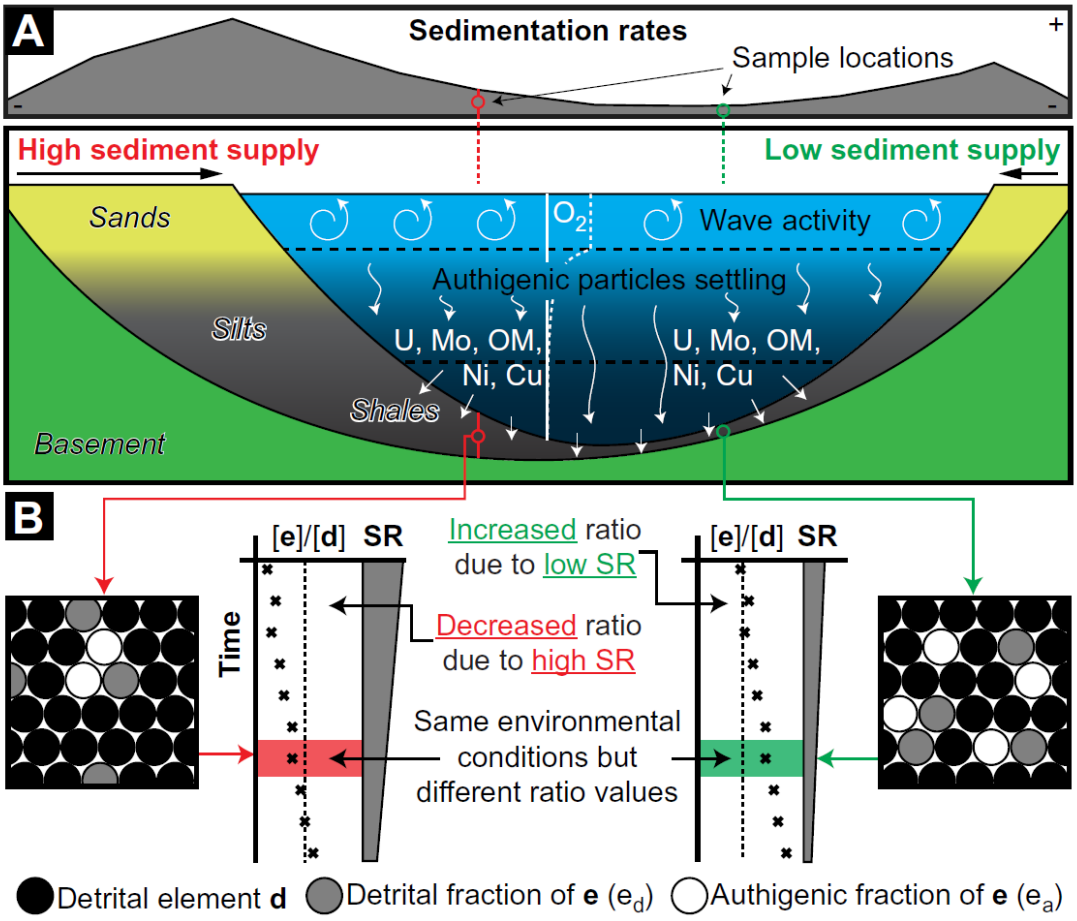

Figure 3. Influence of different sedimentation rates on concentration of authigenic elements. (A) Conceptual basin where sediment supply at each margin is different. (B) Variations in dilution of authigenic elements in two locations, each related to different sediment supplies. OM—organic matter; SR—sedimentation rate.

3. 峨眉山大火成岩省的岩浆作用持续时间：来自越南北部的约束

翻译人：冯婉仪 fengwy@sustech.edu.cn

Shellnutt J G, Pham T T, Denyszyn S W, et al. ***Magmatic duration of the Emeishan large igneous province: Insight from northern Vietnam*** *[J].* ***Geology****, 2020, 48: 457-461. https://doi.org/10.1130/G47076.1.*

摘要：中国西南部和越南北部的峨眉山熔岩的喷发被认为是导致 Capitanian 大灭绝及随后全球变冷事件的一个重要因素，但该火山活动的持续时间不确定。在某些程度上，由于缺乏晚期火山岩的高精度年龄数据使得评估火山活动的停止时间存在困难。越南北部的 Tu Le 流纹岩是峨眉山大火成岩省（ELIP）中体积最大的硅质单元，并且它在空间上与 Muong Hum 和 Phan Si Pan 浅成岩体密切相关。本文对来自 Tu Le 流纹岩（257.1 ± 0.6 Ma 至 257.9 ± 0.3 Ma）以及 Muong Hum（257.3 ± 0.2 Ma）和 Phan Si Pan（256.3 ± 0.4 Ma）浅成岩体的锆石进行了化学研磨-同位素稀释-热电离质谱 U-Pb 定年，并且获得了目前 ELIP 确定的最年轻的高精度年龄。结果表明，峨眉山火山岩的喷发持续了约 6 m.y.，此后不久，侵入岩浆作用就结束了。因此，峨眉山火山作用可能是中吴家坪期全球变冷的原因之一。这些岩石似乎代表了 ELIP 一个独特的岩浆作用时期，因为它们年轻并就位于与南北向攀西裂谷斜交的方向。

ABSTRACT: The eruption of Emeishan lava in southwestern China and northern Vietnam is considered to be a contributing factor to the Capitanian mass extinction and subsequent global cooling event, but the duration of volcanism is uncertain. The difficulty in assessing the termination age is, in part, due to the lack of high-precision age data for late-stage volcanic rocks. The Tu Le rhyolite of northern Vietnam is the most voluminous silicic unit of the Emeishan large igneous province (ELIP) and is spatially associated with the Muong Hum and Phan Si Pan hypabyssal plutons. Chemical abrasion–isotope dilution–thermal ionization mass spectrometry U-Pb dating of zircons from the Tu Le rhyolite (257.1 ± 0.6 Ma to 257.9 ± 0.3 Ma) and Muong Hum (257.3 ± 0.2 Ma) and Phan Si Pan (256.3 ± 0.4 Ma) plutons yielded the youngest high-precision ages of the ELIP yet determined. The results demonstrate that Emeishan lavas erupted over a period of ~ 6 m.y,. with plutonism ending shortly thereafter. Thus, it is possible that Emeishan volcanism contributed to global cooling into the middle Wuchiapingian. It appears that these rocks represent a distinct period

of ELIP magmatism, as they are young and were emplaced oblique to the main north-south–trending Panxi rift.

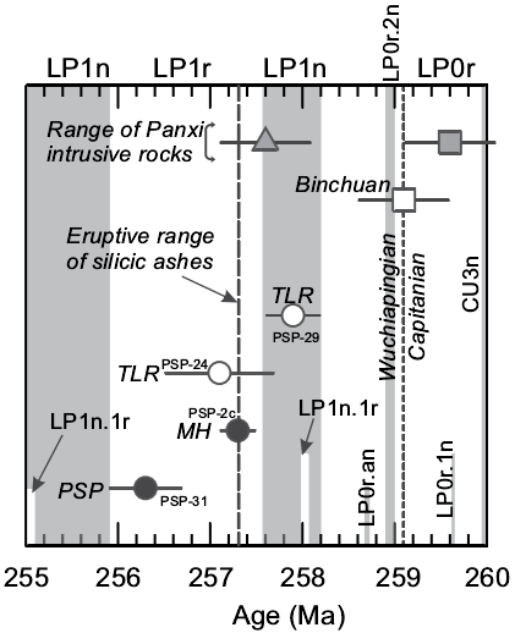

Figure 1. Summary of eruptive and magmatic durations of Emeishan large igneous province (southwestern China and northern Vietnam). The Binchuan ignimbrite (white square; Yunnan, China) was deposited ($^{206}Pb/^{238}U$ = 259.1 ± 0.5 Ma) at the Wuchiapingian-Capitanian boundary (Zhong et al., 2014). The eruptive range (260–257.3 Ma) of silicic ashes is based on Huang et al. (2018) and Mundil et al. (2004). Chemical abrasion–isotope dilution–thermal ionization mass spectrometry (CA-ID-TIMS) $^{206}Pb/^{238}U$ ages (259.6 ± 0.5 Ma to 257.6 ± 0.5 Ma) of Panxi mafic (gray triangle is mafic dike) and silicic intrusive (gray square is Woshui syenite) rocks are from Shellnutt et al. (2012). White circles are the Tu Le volcanic rocks of this study (PSP-29, PSP-24), and black circles are the Muong Hum (PSP-2c) and Phan Si Pan (PSP-31) granitic rocks of this study. Permian geomagnetic polarity time scale magnetochron intervals (labeled gray and white bands) of Hounslow and Balabanov (2016) is added. TLR—Tu Le rhyolite; MH—Muong Hum granite; PSP—Phan Si Pan granite.

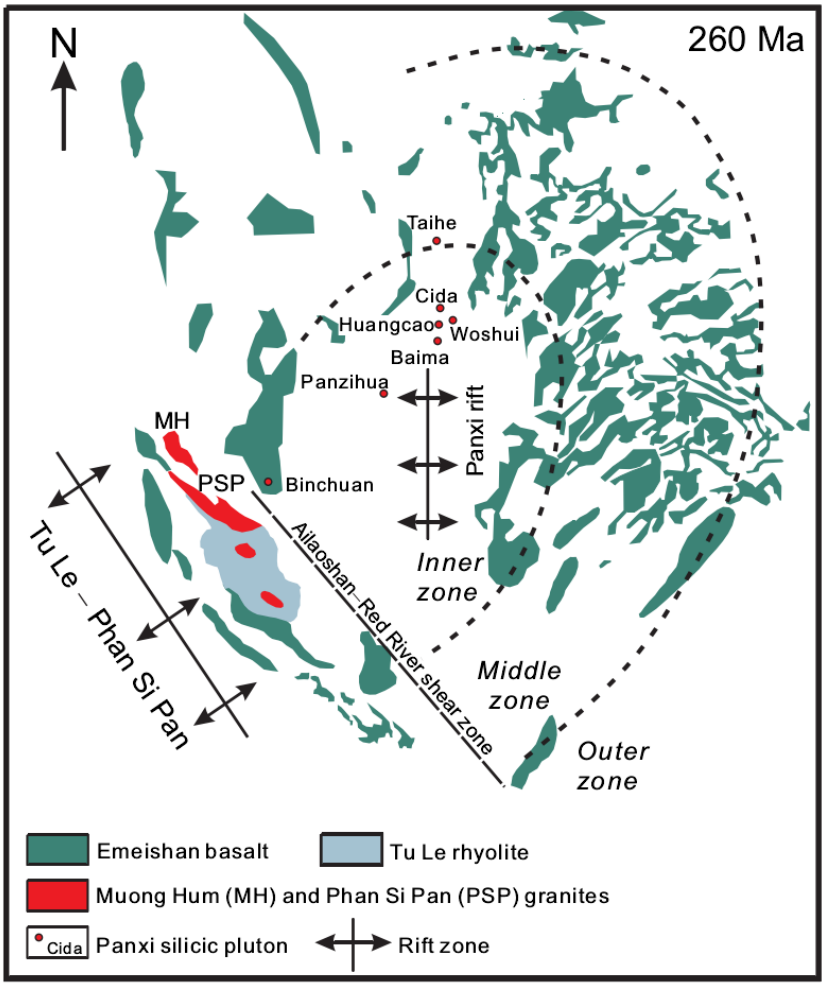

Figure 2. Restored relative paleogeography of the Tu Le–Phan Si Pan region to the inner zone of the Emeishan large igneous province (ELIP; southwestern China and northern Vietnam) by 600 km translation along Ailaoshan–Red River shear zone.

4. Saint Helena 高的古地磁分散度表明南大西洋异常地磁行为长期存在

翻译人:李园洁 liyj3@sustech.edu.cn

Engbers Y A, Biggin A J, Bono R K. ***Elevated paleomagnetic dispersion at Saint Helena suggests long-lived anomalous behavior in the South Atlantic[J]. Proceedings of the National Academy of Sciences****, 2020. https://doi.org/10.1073/pnas.2001217117*

摘要：目前，地球磁场的一个显著特征是南大西洋的异常现象正在不断扩大。地球表面的这一区域是否优先受到地质时期剧烈的地磁场变化的影响，对地核动力学，地核与地幔相互作用以及即将发生的地磁场极性倒转的可能性具有重大影响。本文，我们给出圣海伦娜（Saint Helena）的古地磁数据，圣海伦娜是一个火山岛，非常适合检验在数百万年的时间尺度上，南大西洋异常的地磁场行为的猜测。我们的结果通过了正向烘烤接触检验和倒转检验，得出 8-11 Ma 之间平均方向近似于地心轴向偶极子得到的期望值，但是具有很大的相关方向分散度。这些发现表明，在地质时间尺度上，圣海伦娜附近的地磁长期变化持续增加。反过来，这表明南大西洋作为由地幔相互作用产生的异常地磁行为的场所，同时也似乎降低了当今区域异常是全球极性倒转的先兆的可能性

ABSTRACT：Earth’s magnetic field is presently characterized by a large and growing anomaly in the South Atlantic Ocean. The question of whether this region of Earth’s surface is preferentially subject to enhanced geomagnetic variability on geological timescales has major implications for core dynamics, core-mantle interaction,and the possibility of an imminent magnetic polarity reversal. Here we present paleomagnetic data from Saint Helena, a volcanic island ideally suited for testing the hypothesis that geomagnetic field behavior is anomalous in the South Atlantic on timescales of millions of years. Our results, supported by positive baked contact and reversal tests, produce a mean direction approximating that expected from a geocentric axial dipole for the interval 8 to 11million years ago, but with very large associated directional dispersion. These findings indicate that, on geological timescales,geomagnetic secular variation is persistently enhanced in the vicinity of Saint Helena. This, in turn, supports the South Atlantic as a locus of unusual geomagnetic behavior arising from core-mantle interaction, while also appearing to reduce the likelihood that the present-day regional anomaly is a precursor to a global polarity reversal.

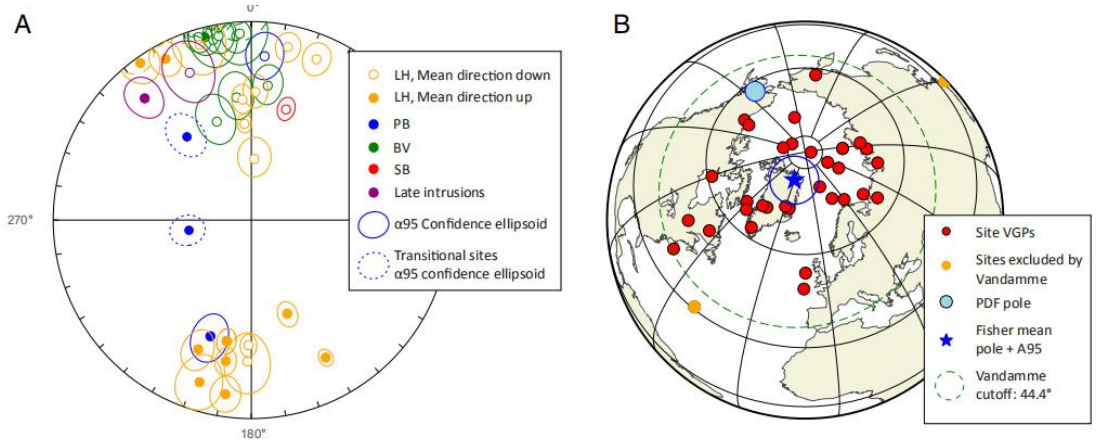

Figure 1. Summary of paleomagnetic data from Saint Helena. (A) The Fisher mean directions per site with a k ⩾ 50 and n ⩾ 5. Transitional [based on the Vandamme cutoff] sites (dashed ellipses) are shown but not used for PSV analysis. (B) Site mean VPGs in red, with the sites excluded by the Vandamme cutoff (44.4°, shown with green dashed line) in orange. The VGP for the PDF is shown in blue. The Fisher mean for all sites with 95% CI are shown with a purple star and purple circle..

5. 相对全新世较低的末次间冰期海洋

翻译人：柳加波

Bengtson S A, Menviel L C, Meissner K J, et al. ***Lower oceanic δ^{13} C during the Last Interglacial compared to the Holocene****[J]. Climate of the Past Discussions, 2020: 1-27.*

https://doi.org/10.5194/cp-2020-73

摘要：地球历史上最后一次高纬度地区比工业革命前温暖的时期是末次间冰期（LIG，129–116 ka BP）。末次间冰期是距离现今最近以及记录最好的温暖期，能够提供在一个更温暖的环境中，气候是如何变化的信息。然而，关于末次间冰期的的一些关键特征目前仍未确立，尤其是关于海洋环流和全球碳循环。针对这两个问题，本文使用 LIG 底栖生物δ^{13}C 的新数据来进行研究。我们发现，与全新世中期（7–4 ka BP）相比，LIG（此处定义为 125–120 ka BP）期间海洋平均δ^{13}C 低了约 0.2‰。由于 LIG 的温度比全新世略高，因此陆源碳可能较低，这可能导致古记录中的海洋δ^{13}C 和大气$\delta^{13}CO_2$ 降低。但是，考虑到千年时间尺度，较低的海洋δ^{13}C 很可能反映出风化和碳埋藏之间的长期不平衡。大西洋中的δ^{13}C 分布表明，在 LIG 和中全新世之间，北大西洋深层水（NADW）的纬度和深度范围没有显著差异。此外，本文数据表明，这两个时间段之间的千年平均 NADW 传输是相似的。

ABSTRACT： The last time in Earth's history when the high latitudes were warmer than during pre-industrial times was the last interglacial (LIG, 129–116 ka BP). Since the LIG is the most recent and best documented warm time period, it can provide insights into climate processes in a warmer world. However, some key features of the LIG are not well constrained, notably the oceanic circulation and the global carbon cycle. Here, we use a new database of LIG benthic δ^{13}C to investigate these two aspects. We find that the oceanic mean δ^{13}C was ~ 0.2 ‰ lower during the LIG (here defined as 125–120 ka BP) when compared to the mid-Holocene (7–4 ka BP). As the LIG was slightly warmer than the Holocene, it is possible that terrestrial carbon was lower, which would have led to both a lower oceanic δ^{13}C and atmospheric $\delta^{13}CO_2$ as observed in paleo-records. However, given the multi-millennial timescale, the lower oceanic δ^{13}C most likely reflects a long-term imbalance between weathering and burial of carbon. The δ^{13}C distribution in the Atlantic Ocean suggests no significant difference in the latitudinal and depth extent of North Atlantic Deep

Water (NADW) between the LIG and the mid-Holocene. Furthermore, the data suggests that the multi-millennial mean NADW transport was similar between these two time periods.

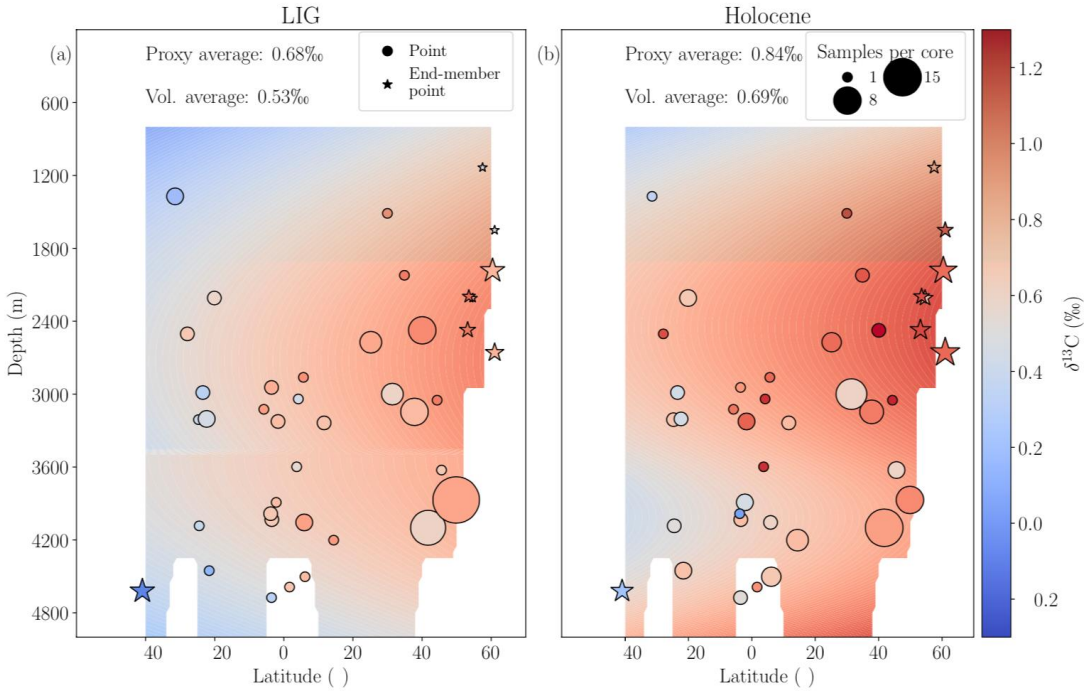

Fig 1: Reconstructed Atlantic $\delta^{13}C$ (‰) meridional section during the LIG and mid-Holocene. The circular points represent the proxy data, showing the average $\delta^{13}C$ with colour and the number of points per core with size. The stars represent the proxy data which make up the end-members. Background shading shows the reconstructed $\delta^{13}C$.

6. 台湾的造山运动----来自三维地球动力学模型的指示

翻译人：刘伟 inewway@163.com

Wang X, Kaus B J, Zhao L, et al. ***Mountain Building in Taiwan: Insights From 3-D Geodynamic Models****[J]. Journal of Geophysical Research, 2019, 124(6): 5924-5950.*

https://doi.org/10.1029/2018JB017165

摘要：台湾一般被认为是被两个极性相反的俯冲带包围的弧-陆碰撞的典型。但两个相邻板块的相互作用是如何引起板块碰撞和造山的，这一点还没有得到充分的理解。人们提出了各种各样的假设，但这些假设在地球动力学上的可靠性还有待检验。本文提出三维热力学模型，来研究台湾的地球动力演化过程。在我们的模型设置中，欧亚板块与南海的边界为东北走向。模拟结果均显示板块边缘存在环向地幔流、板块撕裂伴随地形高峻的小尺度山带和地壳抬升。欧亚大陆地壳以一种穹窿状方式抬升，暴露出较高级的变质岩，这是由高侵蚀率和弱大陆下地壳造成的，但又被弱弧的存在所抑制。地形高峻的造山带和陆壳板片的断离发展成 N307° 方向的汇聚和大的汇聚速率。我们的模型结果与早前基于地震层析结果提出的欧亚大陆板片撕裂模型一致。我们认为快速剥蚀、弱下地壳、快速汇聚和小的汇聚角度等因素的联合作用可以解释台湾造山带的主要特征。

ABSTRACT: Taiwan is widely considered to be a typical example of an arc-continent collision surrounded by two opposite dipping subduction zones. The manner by which the interaction of the two neighboring slabs caused plate collision and mountain building is insufficiently understood. Various hypotheses have been proposed, but the geodynamic feasibility of those remains to be tested. Here we present 3-D thermomechanical models to study the geodynamic evolution process of a Taiwan-like setting after an initial transform fault was consumed. In our model setup, the boundary between the Eurasian plate and the South China Sea is northeast trending. The results show that all simulations result in toroidal mantle flow around the slab edges and that slab breakoff as well as a small-scale mountain belt with high topography and crustal exhumation occurs in most cases. The Eurasian continental crust is exhumed in a dome-like manner exposing higher-grade metamorphic rocks, facilitated by high erosion rates and a weak continental lower crust rheology, but inhibited by the presence of a weak arc. A high topography within the orogen, as well as continental slab detachment, can develop for the convergence direction of N307° and large convergence rates. Our modeling results are thus generally consistent with the Eurasian slab-tearing model proposed for

Taiwan based on seismic tomographic studies, and we suggest that the main characteristic features in Taiwan can be explained by the combined effects of fast erosion, a weak lower crust, fast convergence, and a small convergence azimuth.

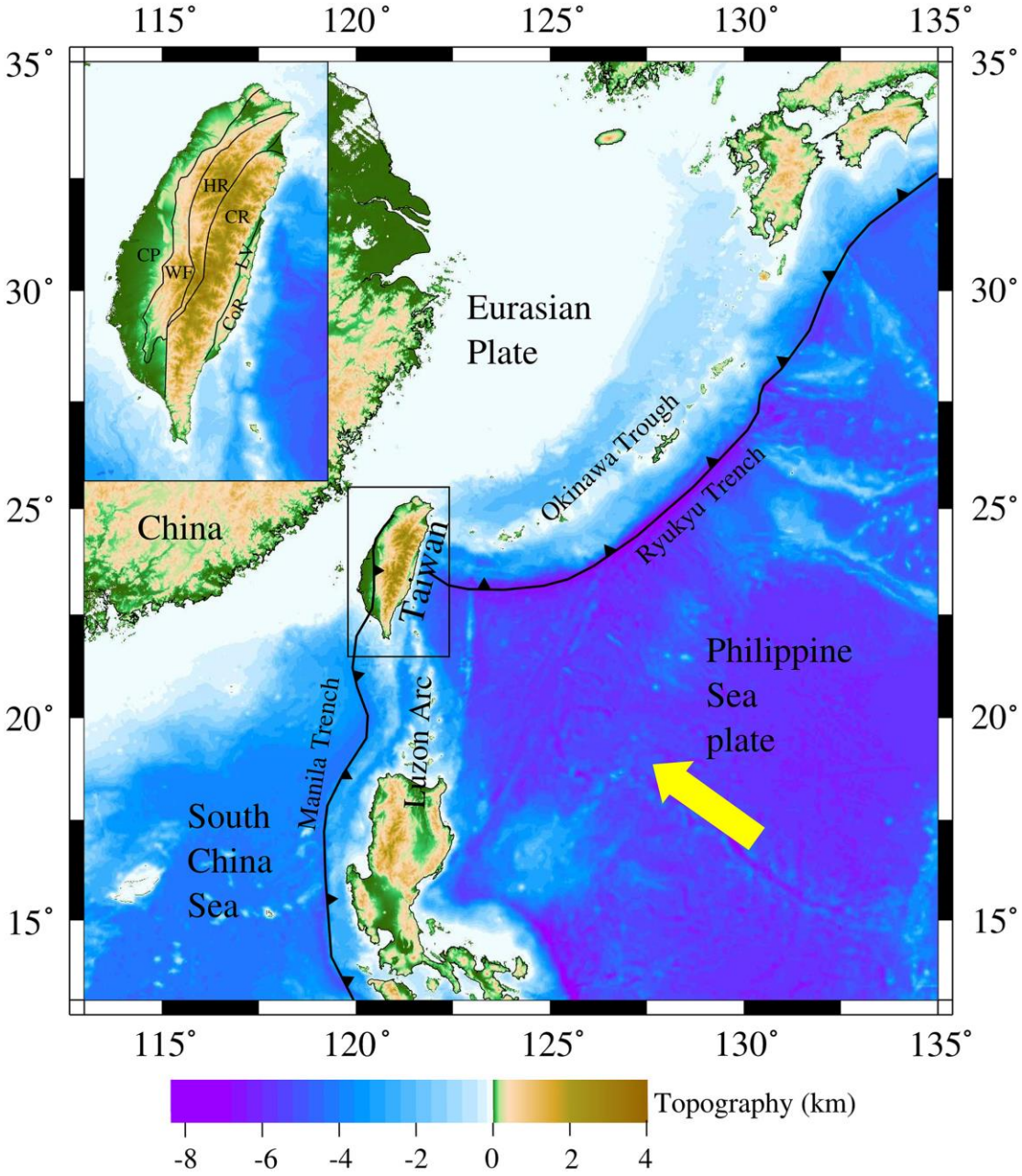

Figure 1. Topographic map of Taiwan and adjacent areas with major tectonic features. The yellow arrow indicates the absolute plate motion of the Philippine Sea plate with respect to the Eurasian plate. The black sawtooth curves denote the Manila trench and Ryukyu trench. The top left inset shows the main tectonic units of the Taiwan orogen. CP = Coastal Plain, WF = Western Foothill, HR = Hsuehshan Range, CR = Central Range, LV = Longitudinal Valley, CoR = Coastal Range.

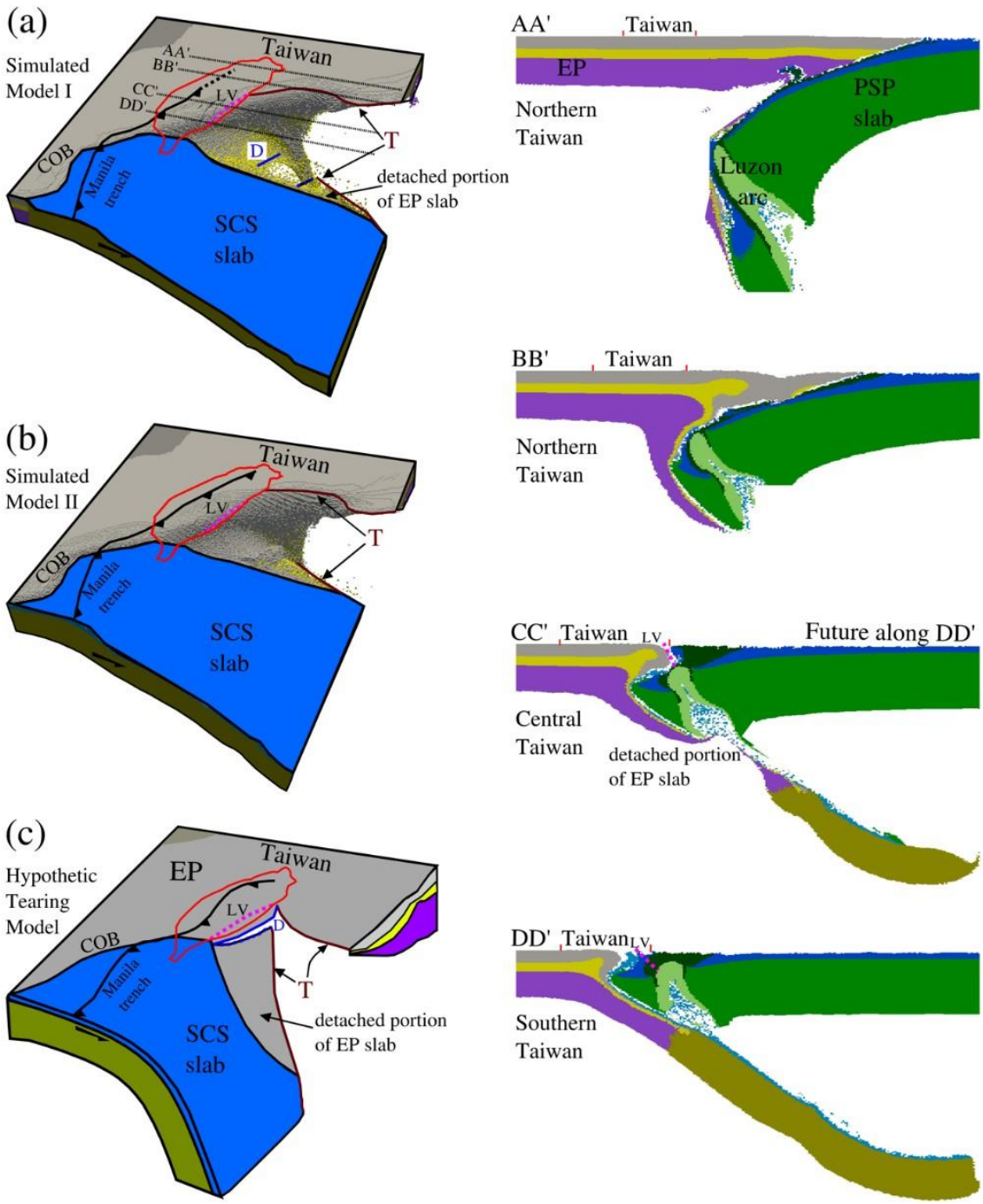

Figure 2. The 3-D perspective view of plate interaction shown in (a) the modeled model I of Taiwan with a constant Philippine Sea plate (PSP) plate velocity in the direction of N307°, (b) the modeled model II of Taiwan in which the convergence direction is N325° in 4 Myr, followed by N305°, and (c) the hypothetic Eurasian plate (EP) slab-tearing model of Taiwan (Lallemand et al., 2001). (AA′–DD′) Cross sections of plate interaction from north to south beneath Taiwan in the modeled model I. T = a tear fault, D = detachment, SCS = South China Sea, LV = Longitudinal Valley, COB = boundary between the Eurasian plate and the South China Sea.

7. 两个穹窿的故事：新近纪至今巴西东北部和非洲西南部的火山活动与动态隆起

翻译人：曹伟

Klöcking M, Hoggard M J, Rodríguez Tribaldos V, et al. ***A tale of two domes: Neogene to recent volcanism and dynamic uplift of northeast Brazil and southwest Africa*** *[J].* ***Earth and Planetary Science Letters****, 2020, 574(1). https://doi.org/10.1016/j.epsl.2020.116464*

摘要：远离板块活动边界的穹窿构造通常具有快速年轻的隆起、同时期的铁镁质火山作用、放射状通道模式以及长波长重力正异常。越来越多的证据表明这些穹窿构造的底部是低异常波速板块，尽管它们的地貌特征众所周知，但这些造陆特征的起源仍然是个谜，并且备受争议。本项研究我们综合分析了来自 Borborema 高原和 Angolan 高原(分别跨越巴西和非洲西南部边缘)的不同观测资料，研究区域快速隆起的潜在机制。我们利用海洋剩余深度测量、水系分析、地层结构、出露海相阶地以及基底剥蚀作用来约束其区域隆升历史。在这两个穹隆区域，大部分地形隆起发生在过去 30 Ma 内，没有明显的构造变形。我们估算了新近纪至今的地幔温度、岩石圈厚度、火山微量元素组成与上地幔横波速度。巴西东北部的火山地球化学资料与软流圈的减压熔融相吻合，可能是岩石圈地幔交代作用的一次次要贡献。在 Angola，交代岩石圈的熔融可能是由小范围软流圈衍生熔体的注入引起的。我们没有发现有证据表明软流圈的热异常比这两个区域下的环境温度高 50 ° C。Angola 现今的岩石圈厚度在 100Km，Borborema 现今的岩石圈厚度可能薄至 60Km。对于 Angola 区域，我们利用白垩纪金伯利岩地幔捕虏体的温度气压来估计古地温梯度。研究表明，在 120Ma 刚果克拉通边缘和安哥拉穹窿中心之间存在一个早期的岩石圈厚度梯度，这个梯度变陡可能是由于穹窿中心以下新近纪额外减薄 30±10 公里的结果。我们得出的结论是 Borberema 和 Angolan 穹窿的新近纪隆起机制是在软流圈中引入一个小的正温度异常，导致上覆岩石圈地幔热机械减薄。

ABSTRACT： Topographic domes that are distant from active plate boundaries are often characterised by rapid, youthful uplift, contemporaneous mafic volcanism, radial drainage patterns, and positive long-wavelength gravity anomalies. There is increasing evidence that they are underlain by anomalously low sub-plate seismic velocities. Despite their well-known geomorphological expression, the origin of these epeirogenic features remains enigmatic and is much debated. Here, we investigate potential mechanisms for rapid regional uplift by combining disparate observations from the Borborema and Angolan plateaux that straddle the Brazilian and

southwest African margins, respectively. Oceanic residual depth measurements, drainage analysis, stratigraphic architecture, emergent marine terraces and basement denudation are used to constrain their regional uplift histories. In both cases, the bulk of topographic growth occurred within the last 30 Ma in the absence of significant tectonic deformation. We estimate present-day mantle temperature and lithospheric thickness from Neogene to recent volcanic trace element compositions and upper mantle shear wave velocities. Volcanic geochemistry in northeast Brazil is compatible with decompression melting of warm asthenosphere and potentially a minor contribution from metasomatised lithospheric mantle. In Angola, melting of metasomatised lithosphere is probably triggered by injection of small-degree asthenospheric-derived melts. We find no evidence for an asthenospheric thermal anomaly >50 °C above ambient beneath either region. Present-day lithospheric thickness is ~100 km beneath Angola and could be as thin as 60 km in the Borborema Province. For Angola, thermobarometry on mantle xenocrysts from Cretaceous kimberlites is used to estimate palaeogeothermal gradients. Results indicate a pre-existing gradient in lithospheric thickness between the edge of the Congo craton and the centre of the Angolan dome at ~120 Ma. This gradient likely steepened as a result of additional Neogene thinning by 30±10km beneath the centre of the dome. We conclude that the mechanism for Neogene epeirogenic uplift of the Borborema and Angolan domes is the introduction of a small positive temperature anomaly into the asthenosphere that causes thermomechanical thinning of the overlying lithospheric mantle.

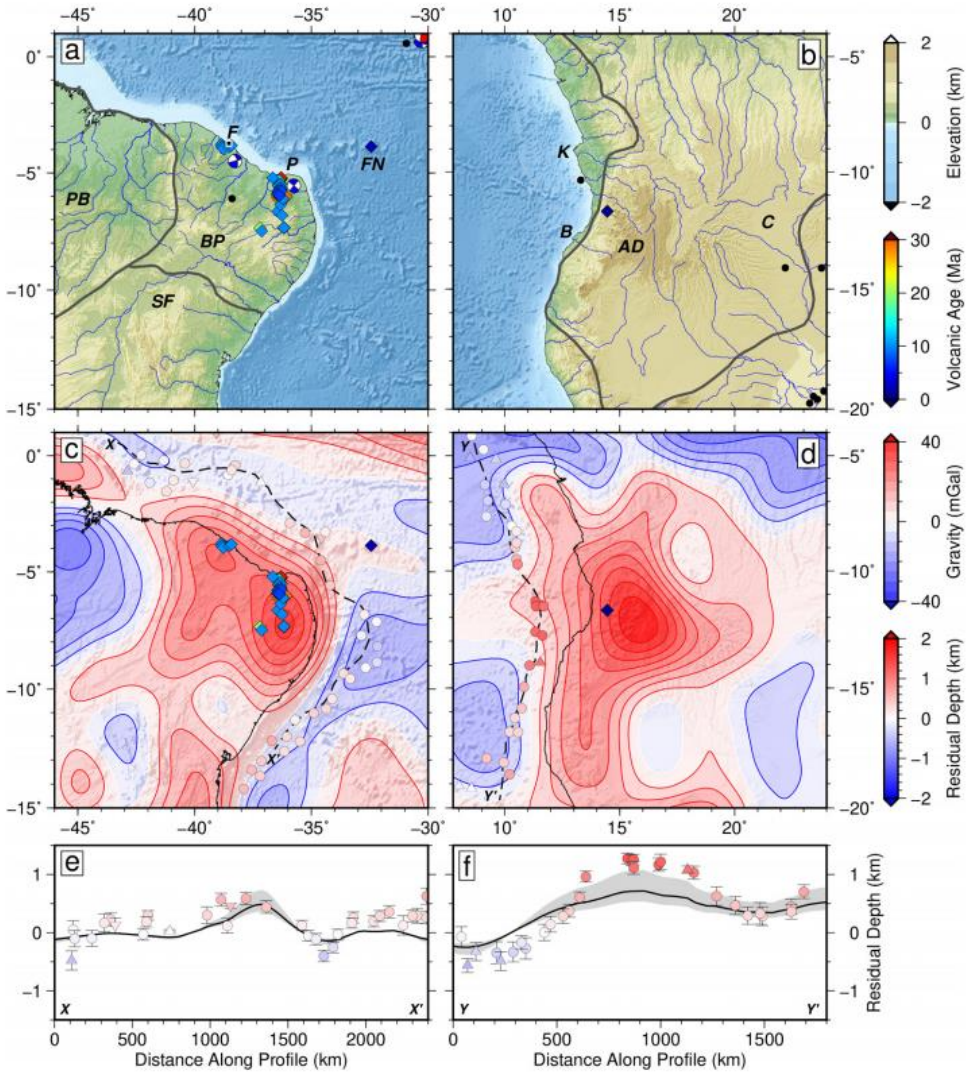

Fig. 1: (a) Topographic map of northeast Brazil. Blue lines = drainage network; black circles = earthquakes of Mw < 5; beachballs = focal mechanisms for earthquakes of Mw > 5; diamonds = volcanic activity <50 Ma, coloured by age in million years (Ma); grey lines = geological province boundaries; BP = Borborema Province; F = Fortaleza; FN = Fernando de Noronha; P = Potiguar basin; PB = Parnaíba basin; SF = São Francisco craton. (b) Same for southwest Africa. AD = Angolan dome; B = Benguela basin; C = Congo craton; K = Kwanza basin. (c) Free-air gravity anomalies in northeast Brazil, bandpass-filtered between 500–4000 km. Coloured circles and up/downward triangles = accurate estimates and lower/upper bounds of oceanic residual depth anomalies ; dashed line = transect shown in (e). (d) Same for southwest Africa; dashed line = transect shown in (f). (e) North-to-south transect offshore Brazil of residual depths within a corridor of 80 km ± 1σ . Black line with grey band = free-air gravity anomalies scaled using admittance, Z=30 ± 10 mGal km−1. (f) Same as (e) for southwest Africa.

8. 从模型角度看亚洲季风起源

翻译人：杨会会 11849590@mail.sustech.edu.cn

Tardif D, Fluteau F, Donadieu Y et al. ***The origin of Asian monsoons: a modelling perspective [J].Climate of The Past,*** *2020, 16, 847–865*

https://doi.org/10.5194/cp-16-847-2020

摘要：亚洲季风在新生代的开始和发展仍然不清楚并引发了许多争论，在过去的几十年里，人们提出了一些关于始新世时期在亚洲起作用的环流模式的假说。其中包括(a)自始新世早期以来，类似于现代季风的季风就已经存在;(b)较弱的南亚季风(SAM)出现，而东亚季候(EAM)几乎没有；热带辐合带(ITCZ)的迁移现象普遍存在，也称为印度尼西亚-澳大利亚季风(I-AM)。一般认为 SAM 和 EAM 最初主要是由亚洲的古地理变化触发或增强的，但它们在动态变化显著的始新世环境中的初现，无论是在建模还是基于野外考查的研究中，仍然是一个悬而未决的问题。我们使用 IPSL-CM5A2 地球系统模型和古地理学研究了始新世亚洲气候条件。我们的始新世气候模拟结果显示，亚洲的大气环流模式与现代条件有很大不同。我们在特提斯洋上方模拟了一个巨大的高压区，由此产生了沿着原始喜马拉雅-青藏高原（HTP）西侧，向南强烈吹拂的低空对流层风。低空风系统阻止了来自印度洋的湿热气团的迁移，使其难以到达 10° N 及更北地区。这与现代的南亚季风形成了鲜明的对比，现代南亚季风将赤道水汽团带至北纬 20-25° N，横跨印度和中国西南地区。本文中始新世模拟的另一个特点是在印度北部的中对流层（约 5000 米）中发生了广泛的下沉，阻止了水蒸汽向上到达冷凝层。这两个过程导致了印度北部和 HTP 广阔地区的干旱。由于 ITCZ 的迁移，降水季节性较强的湿润地区环绕着这个干旱地区。尽管中部干旱地区的存在可能部分是由于我们模拟的特殊性，尚未由地质记录确认，但始新世季风的观测证据大多位于季节性较强的干湿气候过渡区。因此，我们认为，在季风开始之前，亚洲普遍存在带状干旱气候，而季风最有可能发生在始新世古地理变化之后。我们的结果还表明，应该谨慎地使用降水季节性来推断季风环流的存在，而在这个干旱地区收集新的地质证据，对推进这一争议的研究至关重要。

ABSTRACT: The Cenozoic inception and development of the Asian monsoons remain unclear and have generated much debate, as several hypotheses regarding circulation patterns at work in Asia during the Eocene have been proposed in the few last decades. These include (a) the existence of modern like monsoons since the early Eocene; (b) that of a weak South Asian monsoon (SAM) and little to no East Asian monsoon (EAM); or (c) a prevalence of the Intertropical Convergence Zone

(ITCZ) migrations, also referred to as Indonesian–Australian monsoon (I-AM). As SAM and EAM are supposed to have been triggered or enhanced primarily by Asian palaeogeographic changes, their possible inception in the very dynamic Eocene palaeogeographic context remains an open question, both in the modelling and field-based communities. We investigate here Eocene Asian climate conditions using the IPSL-CM5A2 (Sepulchre et al., 2019) earth system model and revised palaeogeographies. Our Eocene climate simulation yields atmospheric circulation patterns in Asia substantially different from modern conditions. A large high-pressure area is simulated over the Tethys ocean, which generates intense low tropospheric winds blowing southward along the western flank of the proto-Himalayan– Tibetan plateau (HTP) system. This low-level wind system blocks, to latitudes lower than 10◦ N, the migration of humid and warm air masses coming from the Indian Ocean. This strongly contrasts with the modern SAM, during which equatorial air masses reach a latitude of 20–25◦ N over India and southeastern China. Another specific feature of our Eocene simulation is the widespread subsidence taking place over northern India in the midtroposphere (around 5000 m), preventing deep convective up draught that would transport water vapor up to the condensation level. Both processes lead to the onset of a broad arid region located over northern India and over the HTP. More humid regions of high seasonality in precipitation encircle this arid area, due to the prevalence of the Intertropical Convergence Zone (ITCZ) migrations (or Indonesian–Australian monsoon, I-AM) rather than monsoons. Although the existence of this central arid region may partly result from the specifics of our simulation (model dependence and palaeogeographic uncertainties) and has yet to be confirmed by proxy records, most of the observational evidence for Eocene monsoons are located in the highly seasonal transition zone between the arid area and the more humid surroundings. We thus suggest that a zonal arid climate prevailed over Asia before the initiation of monsoons that most likely occurred following Eocene palaeogeographic changes. Our results also show that precipitation seasonality should be used with caution to infer the presence of a monsoonal circulation and that the collection of new data in this arid area is of paramount importance to allow the debate to move forward.

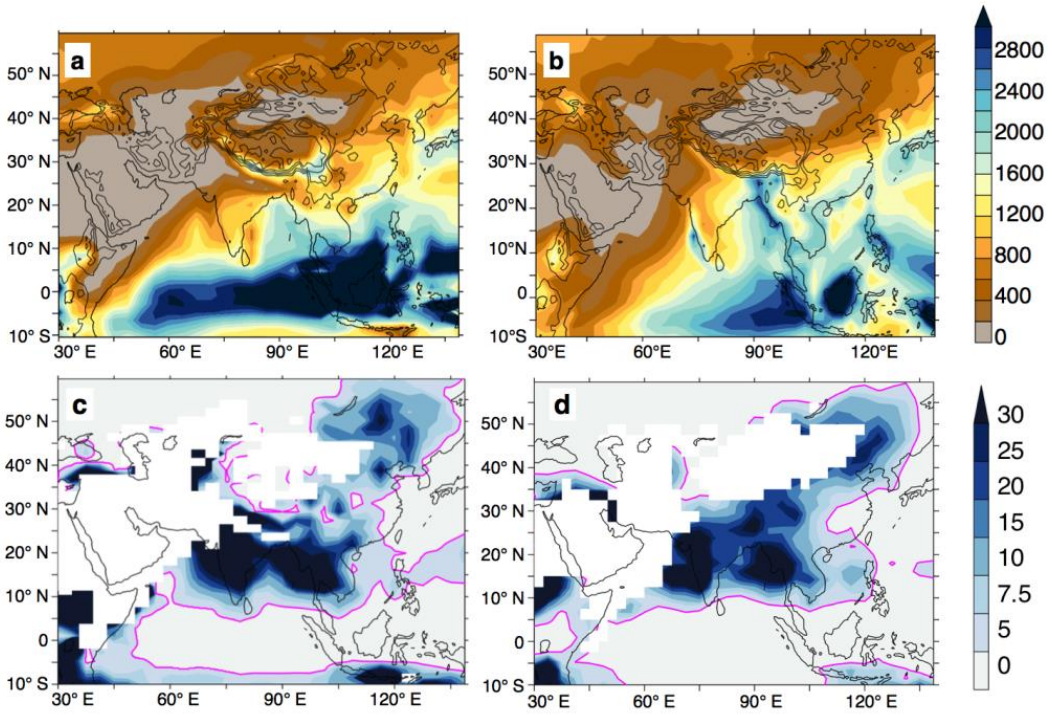

Figure 1. Comparison of (a, b) mean annual precipitations in millimetres per year and (c, d) the 3 wet /3 dry ratio simulated in (a, c) themodern control simulation and (b, d) the GPCP observations.

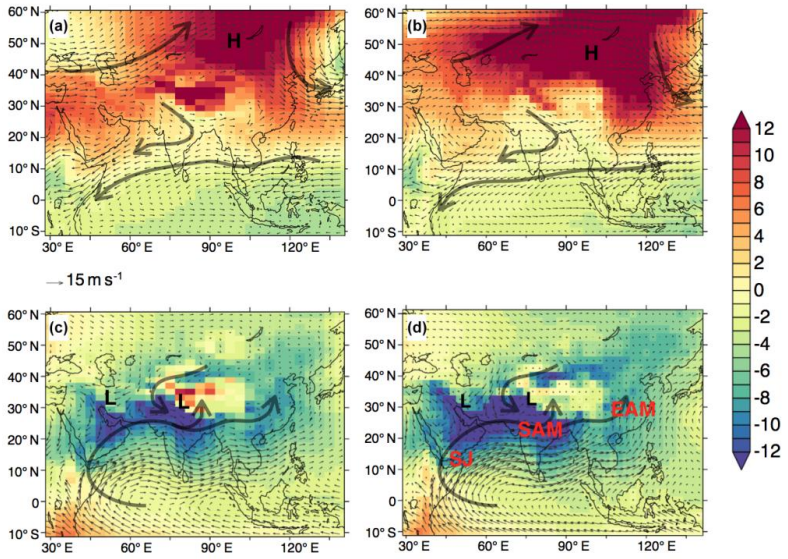

Figure 2. Comparison of (a, b) January to March and(c, d) June to August mean wind patterns obtained (a, c) in the modern control simulation (b, d) with ERA40 reanalysis. Shading represents sea level pressure anomaly (in millibars), calculated as the difference between seasonal SLP minus the mean annual SLP. Overprinted vectors show 850 mbar wind speed expressed in metres per second. Main zones of high (low) pressure are highlighted with H (L) black letters. Main features of the summer monsoon are highlighted in red: Somali jet (SJ), South Asian monsoon (SAM) and East Asian monsoon (EAM).

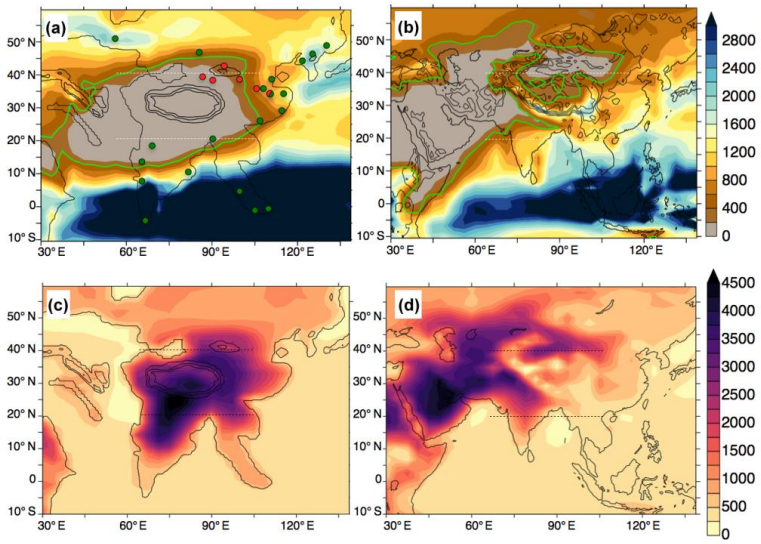

Figure 3. **(a, b)** Mean annual precipitations (mm yr^{-1}) for the **(a)** EOC4X simulation and **(b)** the control simulation. The green outline delimits the arid region receiving less than 1 mm d^{-1}. **(c, d)** Water condensation altitude (in metres) in July for the **(c)** EOC4X simulation and **(d)** control simulation. Horizontal dotted lines show the latitude used for the meridional profiles in Fig. 5. In **(a)**, circles indicate locations of palaeovegetation studies and describe forested environment (green) and shrub/grass environment (red), according to qualitative descriptions described in Table S5.

9. 最近 70 ka 来自马尔马拉海沉积物的高分辨率古地磁记录

翻译人：王浩森 502691781@qq.com

Makaroğlu Ö, Nowaczyk N R, Eriş K K, et al. ***2020. High-resolution palaeomagnetic record from Sea of Marmara sediments for the last 70 ka. Geophysical Journal International [J], 222: 2024-2039.***

doi: 10.1093/gji/ggaa281

摘要：对从马尔马拉海回收的两个沉积岩心进行了磁地层学和地球化学分析，以研究最近 70 ka 期间的地磁场变化。根据八个 AMS 14C 年代，年代学和用格陵兰岛冰芯氧同位素数据中观察到的星际和星际调整 Ca 浓度，为两个岩心中的每个岩心建立了年代学。根据年龄模型，核心 MD01-2430 和 MRS-CS19 分别可恢复到 70 和 32 ka。 MD01–2430 核心的平均沉积速率为 43 cm kyr–1，MRS CS19 核心的平均沉积速率为 68 cm kyr–1，可以高分辨率重建马尔马拉海的地磁场变化。矿物磁特性对该地区的冰川恒流海平面变化和古气候变化敏感，反映了最近 70 ka 期间马尔马拉海古生物环境的变化。尽管由于早期成岩作用，在某些地层间隔中古地磁记录受到了损害，但马尔马拉海沉积物中的相对古强度变化与来自其他地区（例如附近的黑海和 GLOPIS-75 烟囱）的类似记录有很好的相关性。来自马尔马拉海核心的定向记录显示出典型的古生物变化模式，定向异常在 41 和 18 ka，分别代表 Laschamps 和假定的 Hilina Pali 偏移。这两个方向异常也与古强度最小值相关。最低的 34.5 ka 的古强度可能与 Mono 湖的偏移有关，到目前为止，在马尔马拉海的古磁记录中没有记录到方向偏差。

ABSTRACT: Magnetostratigraphic and geochemical analyses were performed on two sediment cores recovered from the Sea of Marmara to investigate geomagnetic field variations over the last 70 ka. A chronology for each of the two cores was developed from eight AMS 14C datings, tephrochronology, and tuning of Ca concentrations with stadials and interstadials observed in Greenland ice core oxygen isotope data. Based on the age models, cores MD01–2430 and MRS-CS19 reach back to 70 and 32 ka, respectively. High average sedimentation rates of 43 cm kyr–1 for core MD01–2430 and 68 cm kyr–1 for core MRS CS19 allow high-resolution reconstruction of geomagnetic field variations for the Sea of Marmara. Mineral magnetic properties are sensitive to

glacioeustatic sea level changes and palaeoclimate variations in this region, reflecting the variable palaeoenvironmental conditions of the Sea of Marmara during last 70 ka. Despite the impairment of the palaeomagnetic record in some stratigraphic intervals due to early diagenesis, relative palaeointensity variations in the Sea of Marmara sediments correlate well with similar records derived from other regions, such as the nearby Black Sea and the GLOPIS-75 stack. The directional record derived from the Sea of Marmara cores exhibits typical palaeosecular variation patterns, with directional anomalies at 41 and 18 ka, representing the Laschamps and postulated Hilina Pali excursions, respectively. Both directional anomalies are also associated with palaeointensity minima. A further palaeointensity minimum at 34.5 ka is likely related to theMono Lake excursion, with no directional deviation documented in the Sea of Marmara palaeomagnetic record so far.

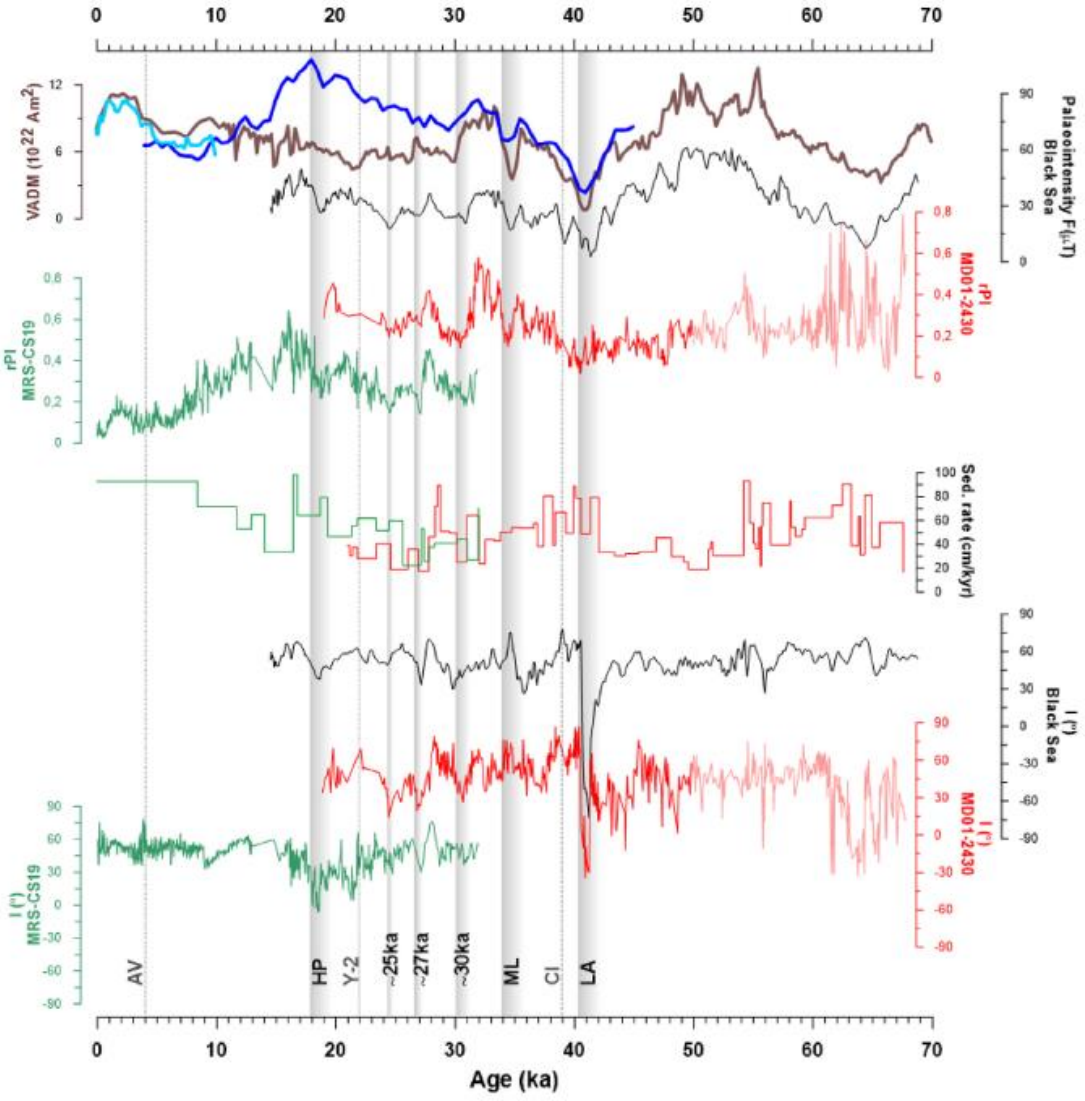

Figure 1. Palaeointensity and inclination records from cores MRS-CS19 (green) and MD01–2430 (red) over the last 70 ka. For comparison, the palaeomagnetic record from the Black Sea (black; Liu *et al.*

subm.), the GLOPIS-75 record (brown; Laj *et al.* 2004), VADM stack (blue; Channell *et al.* 2018), and Holocene model (light blue; Korte *et al.* 2011) are also shown. Light red line shows unreliable RPI record of core MD01–2430. Vertical grey bars denote magnetic field excursions, LA (Laschamps), ML (Mono Lake) and HP (Hilina Pali). The dotted vertical lines mark the stratigraphic positions of the Avellino (AV), Cape Riva (Y-2) and Campanian Ignimbrite tephra (CI/Y-5) in the studied cores.

10. 羌塘北部（西藏）中三叠纪熔岩的古磁性：古特提斯洋封闭的约束

翻译人：李海 Ultimate_LH@cug.edu.cn

Song, P., Ding, L., Lippert, P. C., Li, Z., Zhang, L., & Xie, J. (2020). ***Paleomagnetism of Middle Triassic lavas from northern Qiangtang (Tibet): Constraints on the closure of the Paleo‐Tethys Ocean.*** *Journal of Geophysical Research: Solid Earth, 125, e2019JB017804. https://doi.org/10.1029/2019JB017804*

摘要：作者提供了羌塘地块北部的中三叠纪熔岩的古地磁研究结果，加深对东部古特提斯洋封闭时间和运动学的了解。将 28 个采样点的平均方向划分为 20 个独立的方向组进行迭代计算，结果显示没有岩石重磁化或岩石学证据表明存在风化作用。这些数据为羌塘北部（62.2° N，196.4° E，A_{95} = 5.6° ）建立了中三叠纪第一个基于熔岩的古磁极。将该古地磁极与来自华北地块和塔里木的古地磁极进行了比较，并估计残留的古特提斯洋可能在约 240 Ma 处长达 700 公里。比较羌塘北部与华北北部和塔里木地区的三叠纪纬向历史，表明古特提斯洋的封闭最有可能发生在三叠纪后期。认为羌塘北部地块与 240Ma 左右或之前的古特提斯或伊顿弧之间的大陆碰撞是造成羌塘板块运动的平均速度在~300-240 Ma 期间从~8.5 cm / yr 减速到在~240-210 Ma 期间的~3.6 cm / yr 的主要原因。

Abstract We present results from a paleomagnetic study of Middle Triassic lavas (~242–240 Ma) from the northern Qiangtang block to improve our understanding of the timing and kinematics of the closure of the eastern Paleo-Ocean. Characteristic remanent magnetization directions carried by magnetite and hematite formed during high-temperature oxidation during initial cooling of the lavas are successfully isolated by progressive thermal and alternating field demagnetizations. We bin 28 site mean directions into 20 independent direction groups that pass the fold test, average secular variation, and show no rock magnetic or petrographic evidence of weathering. These data establish the first lava-based paleomagnetic pole of Middle Triassic age for the northern Qiangtang block (62.2°N, 196.4°E, A95 = 5.6°). We compare this pole to coeval poles from the North China Block and Tarim and estimate that the remnant Paleo-Tethys or Hoh-Xil-Songpan-Ganzi Ocean could have been up to 700 km at ~240 Ma. A comparison of the Triassic latitudinal history between the northern Qiangtang block and the North China Block and Tarim shows that the closure of the Paleo-Tethys

Ocean most likely occurred during the latest Triassic. Our review of published Permian-Triassic poles from the northern Qiangtang block show that the average south-north plate velocity of the terrane decelerated from ~8.5 cm/yr during ~300–240 Ma to ~3.6 cm/yr during ~240-210 Ma. We suggest that an arc continent collision between the northern Qiangtang block and a Paleo-Tethys or Yidun arc around or before 240 Ma contributed to this change in plate velocity.

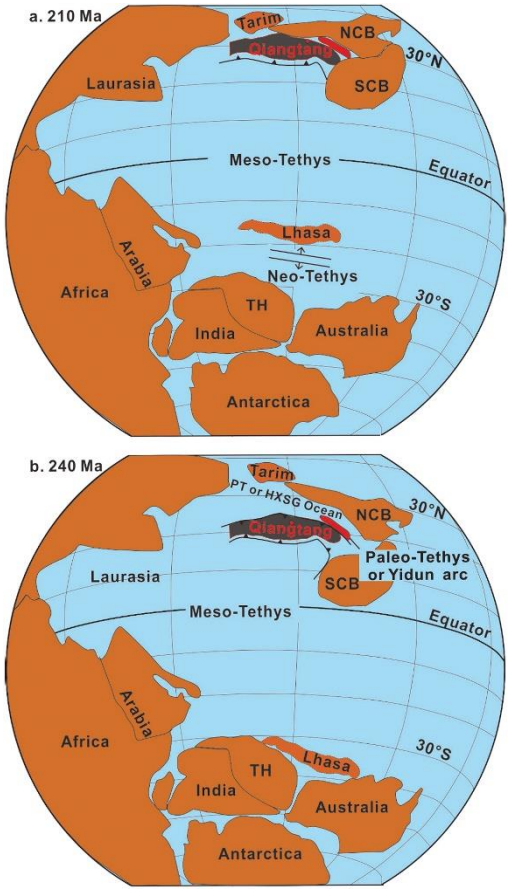

Figure 1. Paleogeography of the northern Qiangtang block in the paleo- magnetic reference frame of Torsvik et al. (2012). Dimensions of the Qiangtang and Lhasa block follow the retrodeformation results presented by van Hinsbergen et al. (2011), while the dimension of the pre-Cretaceous Tethyan Himalaya is based on Ali and Aitchison (2005). The northern Qiangtang block is shown in gray: not that its paleolongitudinal position is unconstrained. SCB: South China block; NCB: North China block; TH: Tethys Himalaya; PT: Paleo-Tethys ocean; HXSG: Hoh-Xil-Songpan-Ganzi basin. (a) Reconstruction for 210 Ma using Qiangtang paleolatitudes from Song et al. (2015). (b) Reconstruction for 240 Ma using the new paleomagnetic results of the Yanshiping lavas described in this paper.